JJAP Series 6
Proc. Int. Symp. on Optical Memory, 1991, pp. 354–358

Holographic Recording in Cerium Doped Strontium Barium Niobate *a*-Axis Single Crystal Fibers

Yasuyuki SUGIYAMA, Shôgo YAGI, Itaru YOKOHAMA[1] and Iwao HATAKEYAMA

NTT Interdisciplinary Research Laboratories, Nippon Telegraph and Telephone Corporation, Tokai, Naka-gun, Ibaraki-ken, 319-11
[1]NTT, Opto-electronics Laboratories, Nippon Telegraph and Telephone Corporation, Wakamiya, Atsugi-shi, Kanagawa-ken, 243-01

(Received August 30, 1991; accepted for publication October 19, 1991)

We have grown cerium doped strontium barium niobate (Ce:SBN60) single-crystal fibers, 250 μm–1 mm in diameter, along the *a*-axis by the laser heated pedestal growth method. The properties of holographic recording in the fiber are investigated. This fiber is expected to have high writing sensitivity due to its large relevant figure of merit and relatively wide grating spacing. The diffraction efficiency reaches more than 40% at 50 ms for a transmitted object beam with an exposure power of 75.2 × 2 μW. The angular sensitivity is 1.5 mrad at an incident angle of 21°. We also demonstrate image recording in the fiber.

KEYWORDS: holographic recording, photorefractive effect, cerium doped strontium barium niobate, single crystal fiber, laser heated pedestal growth, angular sensitivity

§1. Introduction

Photorefractive electro-optic crystals have been extensively studied since they have attractive characteristics for holographic storage,[1–4] optical interconnection, and phase conjugation mirrors.[5–8] In particular, holographic recording using a light-induced change of refractive index (photorefractive effect) in electro-optic crystals such as $LiNbO_3$,[1,2,4] $Sr_xBa_{1-x}Nb_2O_6$ (SBN)[3] was one of the major themes of optical memory research over 15 years ago. There are two important problems related to the implementation of photorefractive crystals in holographic recording systems. One is writing sensitivity which is affected by the electro-optic coefficient and the dielectric constant of the crystal, and also by the dopant in the crystal which supplies photoionized free electrons in the conduction band. Because the photorefractive effect is proportional to the number of absorbed photons, writing is performed more quickly as the power increases. The other is the number of holograms which can be superimposed in a given volume of crystal, and this is limited by angular sensitivity.

In the succeeding years, many researchers have devoted themselves to discovering the mechanism of photorefractive effects[9–12] and developing practical crystals. For example, cerium doped SBN was found to have a high writing sensitivity by Megumi *et al.*[13,14] However, no practical optical memory system using photorefractive crystals has yet been developed, because of the imperfections in the crystals, their very high cost, the lack of a small light source with adequate power and modulation speed at visible wavelengths, and the lack of related components.

Recently, Hesselink *et al.* reported holographic storage in Ce doped SBN *c*-axis fiber and mentioned many advantages of fiber type photorefractive materials.[15,16] Firstly, fiber type crystals are easier to grow than bulk crystals using the laser heated pedestal growth (LHPG) technique.[17–20] Secondly, the angular sensitivity of multiplexed images in fiber increases because the effective interaction length increases due to reflection of the reference beam in the fiber, and each stack of images is isolated from other stacks in adjacent fibers, thereby reducing cross-talk. Moreover, each fiber can be assembled in a variety of configurations. The combined use of photorefractive single crystal fibers and related components, such as the SHG (second harmonic generation) light source, being developed in current studies, will enable a holographic recording system to be realized.

This paper describes the growth of Ce doped SBN single crystal fibers along the *a*-axis by the LHPG technique and also the basic properties of holographic recording with no external field applied to the fiber. Data on holographic grating formation, read-out grating decay and angular sensitivity are presented and image recording in *a*-axis single crystal fiber is demonstrated. These results show that cerium doped SBN *a*-axis fiber can be a holographic recording medium with a higher writing sensitivity than *c*-axis fiber.

§2. Preparation of SBN Single Crystal Fibers

Cerium 0.05% and 0.02% doped $Sr_{0.6}Ba_{0.4}Nb_2O_6$ *a*-axis single crystal fibers grown by the LHPG technique are shown in Fig. 1(a). We have used cerium doped SBN crystal rods about 700 μm-2 mm in diameter and up to 20 mm in length as the source materials. SBN single crystal fibers have been successfully grown along both the *a*- and *c*-axes, with diameters of 100 μm to 1 mm and lengths of up to 40 mm at a speed of a few mm/min. The LHPG technique is described in detail in refs. 17, 18. The fibers, cut to appropriate lengths of 1 to 4 mm, were held with U.V. curing resin and both end-faces were polished. An optical micrograph of the end-face of an SBN *a*-axis single crystal fiber is shown in Fig. 1(b). The cross-sec-

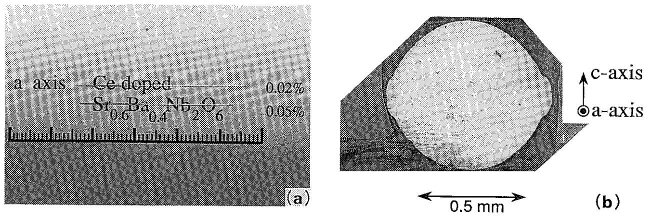

Fig. 1. Photographs of (a) Ce doped *a*-axis single crystal fiber grown by the laser heated pedestal growth technique, (b) the cross-section of prepared Ce doped SBN *a*-axis single crystal fiber. The *c*-axis is perpendicular to the direction of the ridges.

tion of an *a*-axis fiber is hexagonal in shape with two ridges whose direction is perpendicular to the *c*-axis. The crystals are pale yellow and their transparency increases as the cerium concentration decreases. The total absorption and scattering losses in Ce: 0.02% and 0.05% doped SBN fibers were $3.9\,\mathrm{cm}^{-1}$ and $7\,\mathrm{cm}^{-1}$, respectively. Before the photorefractive properties were measured, poling was carried out with a static electric field of more than 500 V/mm along the *c*-axis at an elevated temperature of 80°C.

§3. Measurement System

The system for measuring the photorefractive properties is shown in Fig. 2. An Ar ion laser of $\lambda=514.5$ nm, monochromated with an ethalon, is employed as the light source. The first polarization beam splitter (PBS) is used as an attenuator. The second PBS splits the laser beam into object and reference beams, where the power ratio and the polarization directions of the two beams are altered by the half wave plates located in front of and behind the PBS, respectively. Here, two beams of extraordinary polarization are incident on the fiber, with a crossing angle of $2\theta=21°$ in air, and co-propagate along the *a*-axis, where the *c*-axis is perpendicular to the fiber axis. We define the $+c$ poling direction as the direction from the object beam toward the reference beam before the beams are incident on the fiber, and the opposite direction as the $-c$ poling direction. The object beam is incident on the fiber axis and the reference beam is incident away from the fiber axis. The object and reference beams are focused into the fiber with lenses whose focal lengths are 300 mm and 1000 mm, respectively. The angle between the reference and object beams is changed, without changing the point at which the two beams merge on the front surface of the fiber, by rotating two mirrors with a stage controller through a microcomputer. A silicon photo-detector monitors the power of the transmitted object beam, and its output is stored in a digital oscilloscope. We insert a chopper in the path of the object laser beam and cut the object beam to a sufficiently short duration of 500 μs with the period of 11 ms. By measuring the diffracted beam power in this short time duration, we can precisely monitor the holographic grating formation. The diameters of the object and reference beams are 280 μm and 590 μm, respectively, at the incident plane. Generally, the strongest coupling can be observed when the ratio of the two beams is 1 to 1.[10] The reference beam power is likely to be reduced by reflection at the fiber surface and by scattering at the boundary between the fiber and the resin, and the focused beam diameter of the reference beam is two times larger than that of the object beam, therefore we must increase the reference beam power so that the effective reference beam intensity is equal to that of the object beam. In our experiments, a reference beam power 75 times larger than that of the object beam was required in order to obtain the strongest coupling between object and reference beams. The effective reference beam power for grating formation is regarded as being the same as the object beam power in this paper.

§4. Results and Discussion

4.1 *Grating formation*

Figure 3 shows the time development of diffraction efficiency at the beginning of laser exposure with various object beam powers for a fiber whose cerium concentration, diameter, and length are 0.02%, 700 μm, and 1.5 mm, respectively. The diffraction efficiency is defined as the ratio of diffracted beam power to transmitted object

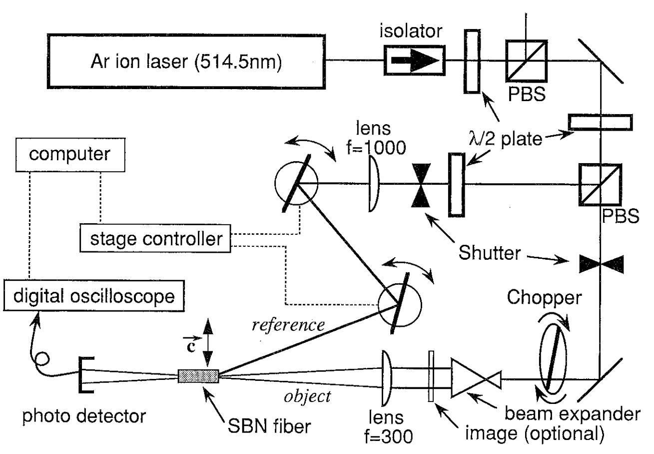

Fig. 2. Experimental configuration for holographic recording. The chopper inserted in the object beam path enables the diffracted beam to be detected during grating formation. The mirrors controlled by the personal computer are used to measure angular sensitivity.

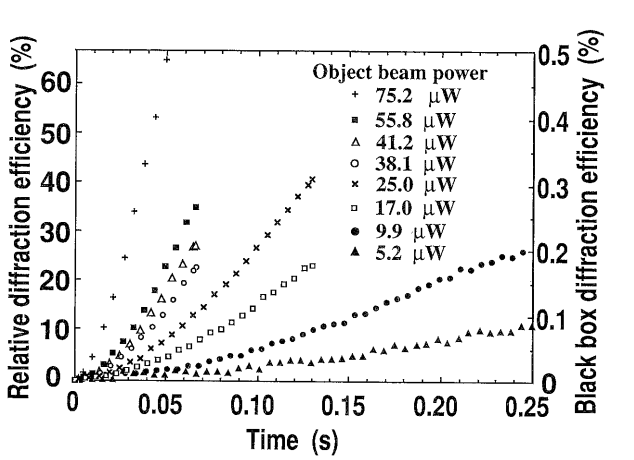

Fig. 3. Relation between diffraction efficiency and time with various exposure powers. $2\theta=21°$. The time development of diffraction efficiency is proportional to the square of time at the very beginning of grating formation.

beam power or to incident reference beam power (black box diffraction efficiency). Each diffraction efficiency develops in proportion to the square of the exposure time at the very beginning of the exposure in an object beam power range of 5.2–75.2 μW. The writing speed is rather fast, and depends on the writing intensity. The diffraction efficiency for the transmitted object beam reaches more than 40% at 50ms with an exposure power of 75.2×2 μW. According to the Kogelnik's theory,[21] the diffraction efficiency, η, is expressed as

$$\eta=\exp\left(-\frac{\alpha d}{\cos\theta}\right)\sin^2\left(\frac{\Delta n\pi d}{\lambda\cos\theta}\right), \quad (1)$$

$$\Delta n=-\frac{1}{2}n^3 r_{ij}E_{sc}, \quad (2)$$

where α is the absorption coefficient, Δn is the refractive index change, λ is the wavelength of light, d is the length of the crystal, 2θ is the cross angle between object and reference beam, n is the refractive index, r_{ij} is the electro-optic coefficient, and E_{sc} is the space charge field in the crystal. E_{sc} is directly proportional to the product of the light intensity and the time during which the light was exposed,[10] namely proportional to the energy used. Then the diffraction efficiency, η, is proportional to the square of the time at the beginning of grating formation. Our results obtained with real-time monitoring by means of the chopper inserted in the object beam path agree with this theory very well at the very beginning of grating formation.

4.2 *Writing sensitivity*

In Fig. 4 we plot the values of $\sqrt{\eta}/t$ against the exposure power (2×object beam power), where t is the grating formation time. The values of $\sqrt{\eta}/t$ which relate to writing speed are obtained from the slope of the linear function between $\sqrt{\eta}$ and time at the very beginning of grating formation. In two experiments with different poling directions ($+c$ and $-c$), there was little difference in the writing speed. The writing speed increases linearly with increases in exposure power.

The writing sensitivity, S_η, at the beginning of grating formation is defined as

$$S_\eta=\frac{\partial\sqrt{\eta}}{\partial(\alpha W)}\frac{1}{d}, \quad (3)$$

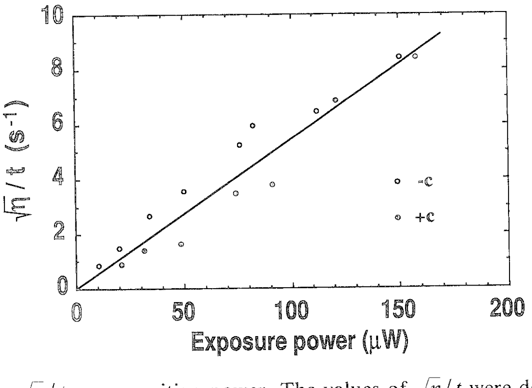

Fig. 4. $\sqrt{\eta}/t$ versus writing power. The values of $\sqrt{\eta}/t$ were derived from the slope of the linear function between $\sqrt{\eta}$ and time at the very beginning of grating formation.

where W is the effective intensity for generating a grating.[10] Then, we can obtain the value of $S_\eta^{-1}=17$ mJ/cm^2, which is derived from the slope of the line in Fig. 4, the values of $\alpha=3.9$ cm^{-1}, $d=0.15$ cm and the beam area of 6.2×10^{-4} cm^2. This value is fairly good compared with other reported values such as 15 mJ/cm^2 in Ce:SBN and 50–1000 mJ/cm^2 in $BaTiO_3$ and $LiNbO_3$.[10] There is another possible way to improve writing sensitivity. Cerium ions are photoionized by means of the reaction:[22]

$$Ce^{3+}+h\nu\rightarrow Ce^{4+}+e^- \text{ (conduction band)}, \quad (4)$$

therefore, the number of cerium atoms which occupy the Ce^{3+} state is more important than their concentration. Namely the valence state of the dopants contributing to the photoionization process is more important than the dopant concentration in the crystal. Actually, we can not observe much difference in writing sensitivity between 0.05% and 0.02% Ce doped crystals. In addition, when the crystals were annealed their writing sensitivity was greatly reduced in our primary experiments. Therefore, control of the valence state of the dopant will be the key to further improvements in writing sensitivity.

4.3 *Readout grating decay*

Figure 5 shows readout decay curves for various reading reference beam powers for the experiment where $-c$ poling was used. This experiment and the measurements of the grating formation process were carried out simultaneously. The maximum diffraction efficiency at each initial state is different, and so the diffraction intensity is normalized by the initial value for each reading power. Each diffraction efficiency exhibits exponential decay. Figure 6 shows the power dependence of the decay rate which is defined as the inverse of the time during which the initial diffraction intensity falls by $1/e$. The reading power is considered to be the same as the object beam power so as not to underestimate the decay rate although the reference beam power is actually 75 times larger than the object beam power before they are incident on the fiber. The 40 μW decay rate is 10 s^{-1} for $-c$ poling. The decay rate increases linearly with increases in

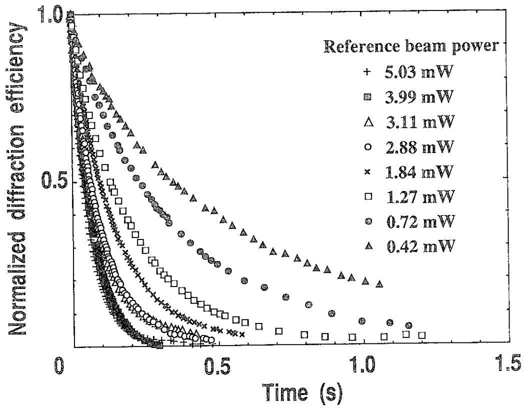

Fig. 5. Readout grating decay curve for various reading powers. Note that the powers indicated in the graph are the actual reference beam powers before being incident on the fiber and the effective reference beam power is considered to be the same as the object beam power.

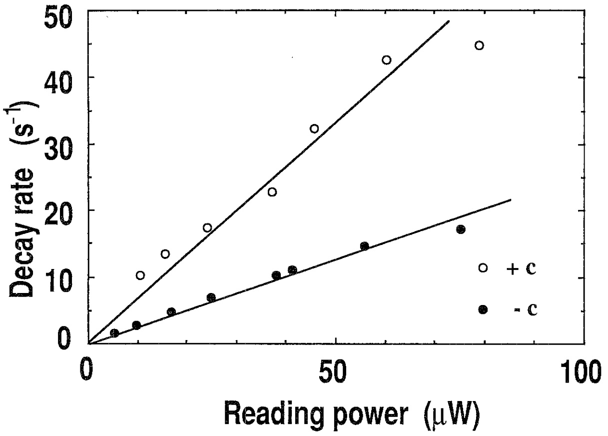

Fig. 6. The relation between decay rate and reading power. Reading power is considered to be the same as the object beam power. $+c$ and $-c$ represent opposite poling directions which relate to the arrangement of the two beams.

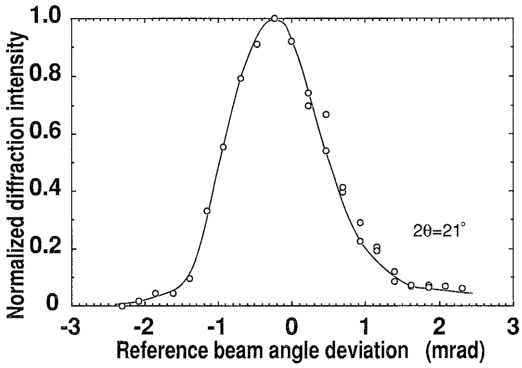

Fig. 7. Relation between diffraction intensity and reference (reading) beam angle deviation. The angular sensitivity defined as the half width of the spectrum is 1.5 mrad.

reading power, and the decay rate for $+c$ poling is 2.7 times larger than that for $-c$ poling.

In a volume hologram, the reading beam can interfere with its own diffracted beam. With photorefractive volume holograms, the reading beam interferes constructively or destructively with its own diffracted beam, because there is a phase shift between the light interference pattern and the recorded grating.[10] This is because a dynamic energy redistribution occurs between the two recording beams during the grating formation process. This means that one beam gains power from the other beam. When we read the hologram stored in the crystal, reversing the poling direction causes the beam to either gain or lose power. Therefore, we observe a slower decay rate with $-c$ poling, where the diffracted beam gains power from its reading beam in the same manner as the writing grating, than with $+c$ poling. The decay rate we obtained, however, is unexpectedly fast even with $-c$ poling. The value of $10\,s^{-1}$ at 40 μW reading power is faster than that of bulk crystal. The corresponding erasure sensitivity of 6.5 mJ/cm^2 is rather higher than the reported value of 30–40 mJ/cm^2.[14] This difference in decay rate is not presently understood. Imperfect poling in the fiber crystal may affect this difference.

4.4 *Angular sensitivity*

Figure 7 shows the angular sensitivity at the cross angle of 21°. The angle of the readout reference beam is precisely changed from left to right by 2 mrad on the basis of the writing angle of the reference beam. The angular sensitivity shown by the half width of this curve is 1.5 mrad. According to Kogelnik's theory,[21] the angular sensitivity can be approximated by

$$\Delta\theta \approx \frac{\Lambda}{d} = \frac{\lambda}{2d\sin\theta}, \tag{5}$$

where, $\Delta\theta$ is the spectral bandwidth where diffraction intensity falls by 1/2, Λ is the grating spacing, and λ is the wavelength. In our case, the calculated value of $\Delta\theta$ is 0.94 mrad with $\lambda=514.5$ nm, $\theta=10.5°$, $d=1.5$ mm. The measured value is slightly larger than the theoretical one. This is due to the beam divergence resulting from the use of a focused laser beam and the low optical quality of the crystal fiber.

The recording density in volume holographic memory is related to the number of holograms which can be superimposed in a given volume of the crystal, and this is limited by angular sensitivity. With an angular sensitivity of 1.5 mrad and a 1.5 mm long fiber, in principle more than 500 holograms can be superimposed with an angular variation of 45° in one dimension in a fiber less than 1 mm in diameter. The merit of the fiber type hologram is the improvement in angular sensitivity due to the lengthening of the effective interaction length by means of multireflection in the fiber. When we use a 1 cm-long fiber, more than 3000 holograms can be superimposed in the fiber. It should be noted that we must determine the optimum dopant concentration so as to fulfill the requirements for both writing sensitivity and superimposition, since the diffraction efficiency decreases due to light absorption with increases in fiber length.

4.5 *Image recording*

Figure 8 shows a reconstructed image stored in Ce:0.05% doped SBN fiber, with a diameter of 250 μm and a length of 1 mm. A chromium coated image mask,

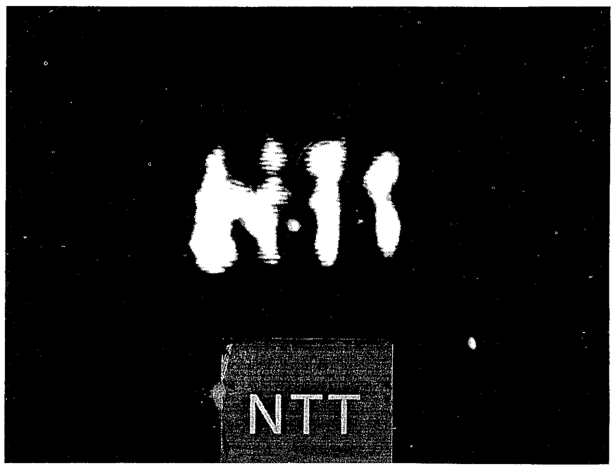

Fig. 8. Reconstructed image of 'NTT', stored in a Ce doped SBN a-axis single crystal fiber, 250 μm in diameter and 1 mm long.

5 × 10 mm in size, was inserted in the object beam path. The reconstructed image quality is rather bad. The SBN fiber we used had a crack in the direction perpendicular to the *c*-axis and seemed to have considerable internal stress based on observation with a polarizing microscope, therefore even the transmitted image quality without beam coupling was rather bad. The scattering on the surface between the SBN fiber and the surrounding resin also may have spoiled the image quality. The removal of internal stress to improve image quality could be one of the most important areas of work on the growth of photorefractive single crystal fiber.

4.6 *Comparison with c-axis fiber hologram*

The SBN crystal has large electro-optic coefficients of r_{33} and r_{13}. This means that the grating vector must be parallel or almost parallel to the *c*-axis to obtain a larger photorefractive effect. Therefore, laser beams must be input into the *a*-axis fiber from the same side (co-propagating type) and into the *c*-axis fiber from the opposite side (counter-propagating type). In such arrangements, we can effectively use the electro-optic coefficient of r_{33} in the *a*-axis fiber and r_{13} in the *c*-axis fiber. The relevant figure of merit Q $(=r_{\mathrm{eff}}/n_{\mathrm{r}}\varepsilon)$ of the *a*-axis fiber is larger than that of the *c*-axis fiber, mainly because r_{33} is about four times larger than r_{13}, where r_{eff}, n_{r} and ε are the relevant electro-optic coefficient, relevant refractive index and relevant dielectric constant, respectively.[23-26]

Moreover the grating spacing of a *c*-axis fiber hologram is much smaller (typically less than 0.15 μm) than that of an *a*-axis hologram (typically more than 1 μm). With such a difference in the grating spacing, the space charge field in the *c*-axis fiber is smaller than that in the *a*-axis fiber.[27] Since larger figures of merit and the larger space charge fields produce larger refractive index changes, as shown in equations (1), (2), the writing sensitivity in *a*-axis fiber should be superior to that of *c*-axis fiber. Actually, Q is about two times larger in *a*-axis fiber than in *c*-axis fiber in our calculation, and the experimental results show that the grating formation speed is four times faster than that of *c*-axis fiber.[26] In addition, an external electric field, which leads to improved writing sensitivity, is easily applied to *a*-axis crystal fiber perpendicular to the light propagating direction, and the required applied voltage is about 1 order less than that required for *c*-axis fiber.

On the other hand, the superimposition in *a*-axis fiber is inferior to that in *c*-axis fiber because we can use all solid angles for writing in the *c*-axis fiber due to the unique arrangement between the *c*-axis and both two writing beams, independent of incident solid angles. In the *a*-axis fiber, however, only one direction, the *c*-axis direction, can be used effectively. The choice of fiber will depend on the system employed.

§5. Conclusion

We grew *a*-axis SBN single crystal fibers by the laser heated pedestal growth method. The grating formation process was successfully analyzed by means of a method using a chopper inserted object beam path. We found that the writing sensitivity and the angular sensitivity in the fiber was fairly good, but the decay rate was unexpectedly fast. Further investigation to improve fiber crystal quality, mainly by reducing internal stress, is required to refine image quality. The results show that cerium doped SBN *a*-axis single crystal fiber can be used as a holographic recording medium with high writing sensitivity.

Acknowledgements

The authors would like to thank Dr. K. Kubodera, Dr. G. M. Davis, Dr. S. Sudo, Mr. Y. Nishida and Mr. K. Nonaka for helpful discussions. The authors also acknowledge Dr. T. Sugeta and Dr. Y. Ishii for their encouragement.

References

1) F. S. Chen, J. T. LaMacchia and D. B. Fraser: Appl. Phys. Lett. **13** (1968) 223.
2) E. Okamoto, H. Ikeo and K. Muto: Appl. Opt. **14** (1975) 2453.
3) J. B. Thaxter and M. Kestigian: Appl. Opt. **13** (1974) 913.
4) D. L. Staebler and J. J. Amodei: J. Appl. Phys. **43** (1972) 1042.
5) A. Yariv, J. AuYeung, D. Fekete and D. M. Pepper: Appl. Phys. Lett. **32** (1978) 635.
6) J. Feinberg and R. W. Hellwaeth: Opt. Lett. **5** (1980) 519.
7) J. Feinberg and R. W. Hellwaeth: Opt. Lett. **6** (1981) 257.
8) J. Feinberg: Opt. Lett. **7** (1982) 486.
9) C. Medrano, E. Voit, P. Amrhein and P. Günter: J. Appl. Phys. **64** (1988) 4668.
10) *Photorefractive Materials and Their Applications I*, eds. P. Günter and J. P. Huignard (Springer-Verlag, Berlin, 1988) Chap. 2, p. 7.
11) F. P. Strohkendl, P. Tayebati and R. W. Hellwarth: J. Appl. Phys. **66** (1989) 6024.
12) M. D. Ewbank, R. R. Neurgaonkar and W. K. Cory: J. Appl. Phys. **62** (1987) 374.
13) K. Megumi, N. Nagatsuma, Y. Kashiwada and Y. Furuhata: J. Mat. Sci. **11** (1976) 1583.
14) K. Megumi, H. Kozuka, M. Kobayashi and Y. Furuhata: Appl. Phys. Lett. **30** (1977) 631.
15) L. Hesselink and S. Redfield: Opt. Lett. **13** (1988) 877.
16) L. Hesselink: Int. J. of Optoelectronics **5** (1990) 103.
17) M. M. Fejer, J. L. Nightingale, G. A. Magel and R. L. Byer: Rev. Sci. Instrum. **55** (1984) 1791.
18) R. S. Feigelson: J. Cryst. Growth **79** (1986) 669.
19) J. K. Yamamoto and A. S. Bhalla: Mat. Res. Bull. **24** (1989) 761.
20) S. Sudo and I. Yokohama: *7th Int. Symp. on the Applications of Ferroelectrics* (1990) 5.2.
21) H. Kogelnik: Bell. Syst. Tech. J. **48** (1969) 2909.
22) R. R. Neurgaonkar and W. K. Cory: J. Opt. Soc. Am. **B/3** (1986) 274.
23) J. Feinberg: J. Opt. Soc. Am. **72** (1982) 46.
24) P. Yeh: Appl. Opt. **26** (1987) 602.
25) P. Yeh: IEEE. J. Quantum Electron. **QE-25** (1989) 484.
26) Y. Sugiyama, I. Yokahama, K. Kubodera and S. Yagi: IEEE. Photo. Tech. Lett. **3** (1991) 744.
27) G. A. Rakuljic, A. Yariv and R. R. Neurgaonkar: Opt. Eng. **25** (1986) 1212.